Completely Capturing Light Pulses in a Few Dynamically Tuned Microcavities

Clayton Ryan Otey, Michelle L. Povinelli, and Shanhui Fan, *Senior Member, IEEE, Fellow, OSA*

***Abstract*—We describe a dynamically tuned system capable of capturing light pulses incident from a waveguide in a pair of microcavities. We use coupled mode theory to design a method for determining how to tune the microcavity resonant frequencies. The results show that pulses can be captured almost completely, with arbitrarily small reflected power. We optimize the pulse capture bandwidth by varying the cavity coupling constants and show that the maximum bandwidth is comparable to the resonant-frequency tuning range. Our system may be implemented using refractive-index tuning in a 2-D silicon photonic crystal slab. Current technology would allow for capture of pulses with widths as low as ~100 ps, with a holding time limited only by cavity loss rates.**

***Index Terms*—Coupled mode analysis, optical pulses, optical resonators, simulation, waveguides.**

I. Introduction

THE ability to stop light on chip has potential applications in all-optical information processing, such as buffering, and enhancement of nonlinear effects [1] for signal processing [2]. In previous work, Yanik *et al.* have shown that dynamic tuning processes are required for stopping light pulses [3], [4]. They designed a dynamic process for a photonic crystal system of coupled microcavities that captures pulses by reversibly compressing the system bandwidth. In their system the capture process is independent of pulse shape. However, their design necessitates the use of many microcavities [3]–[9].

This initial theoretical work has motivated experiments with simpler, more experimentally accessible systems containing fewer resonators. Xu *et al.* used a pair of silicon ring resonators with dynamically tuned resonance frequencies to capture and delay portions of pulses [10]. Tanaka *et al.* have also demonstrated dynamic control of the Q factor of photonic crystal nanocavities [11]. The question naturally arises as to whether these few-cavity systems are capable of *completely* capturing pulses.

For macroscopic systems, it has been shown [12] that light pulses can be completely captured in a single resonator. Arbitrarily long pulses can be captured without reflection by tuning the reflectivity of one of the cavity mirrors. However, such a tuning mechanism is typically not available in on-chip devices, where one generally tunes the cavity resonant frequency instead.

In this paper, we show that resonant frequency tuning can be used to completely transfer a pulse from an input waveguide into a few cavities, capturing the pulse without reflection. Essential to the scheme is the existence of a "dark" state decoupled from the waveguide, and a tuning process that transfers energy from the waveguide into the dark state. In Section II, we provide a numerical demonstration of pulse capture. We then employ a time-reversal argument to recast the pulse capture problem as a pulse release problem. We show that by tuning just one cavity, only chirped pulses may be captured or released, whereas by antisymmetricaly tuning two cavities, unchirped pulses may be captured or released.

In Section III, we describe how to determine the tuning process required to capture a pulse of a given shape with negligible reflection. General features of the dynamics in the adiabatic (slow tuning/long pulse) and nonadiabatic (fast tuning/short pulse) limits are discussed in Section IV. Section V shows how the system parameters may be designed to optimize the pulse bandwidth. We conclude with a brief description of a buffer design and practical considerations for the experimental implementation of the pulse capture system.

II. Demonstration

We first numerically demonstrate the complete capture of a light pulse in a system of a few cavities using coupled mode theory. Specifically, we consider three cavities with resonant frequencies ω_0, ω_1, and ω_2, coupled to each other with coupling constant β and to a waveguide with coupling constant γ. The system is shown schematically in Fig. 1. Incomplete pulse capture in similar systems has previously been described in [13]. For ease of simulation, we initially assume that the waveguide is a coupled resonator optical waveguide (CROW) [14], [15] with inter-cavity coupling constant α, shown schematically in Fig. 2. The three-cavity system is coupled to the CROW with coupling constant δ. In Section IV we will argue that the relevant dynamics are independent of the details of the CROW design, and we will explore the dynamics in a more general setting.

Assuming that the Q of the cavities is sufficiently large, we may accurately model the CROW-coupled system with the following equations for the complex field amplitudes in each cavity:

$$\begin{aligned}
\frac{da_0}{dt} &= i\omega_0 a_0 + i\beta a_1 + i\beta a_2 + i\delta a_3 \\
\frac{da_1}{dt} &= i\omega_1(t) a_1 + i\beta a_0 \\
\frac{da_2}{dt} &= i\omega_2(t) a_2 + i\beta a_0 \\
\frac{da_3}{dt} &= i\omega_0 a_3 + i\delta a_0 + i\alpha a_4 \\
\frac{da_m}{dt} &= i\omega_0 a_m + i\alpha a_{m-1} + i\alpha a_{m+1}, \qquad m = 4 \ldots M. \quad (1)
\end{aligned}$$

Manuscript received April 15, 2008; revised August 01, 2008 and August 27, 2008. Current version published January 28, 2009. This work was supported in part by the United States Air Force Office of Scientific Research (AFOSR) under Grant FA9550-05-0414 as part of the DARPA DSO Slow Light Program and by the Packard Foundation.

The authors are with the Edward L. Ginzton Laboratory, Stanford University, Stanford, CA 94305 USA (e-mail: otey@stanford.edu; mpovinel@stanford.edu; shanhui@stanford.edu).

Color versions of one or more of the figures in this paper are available online at http://ieeexplore.ieee.org.

Digital Object Identifier 10.1109/JLT.2008.2005511

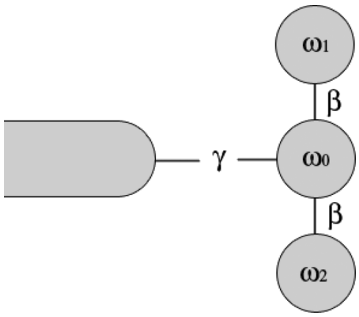

Fig. 1. Three-cavity system coupled to a waveguide with coupling constant γ.

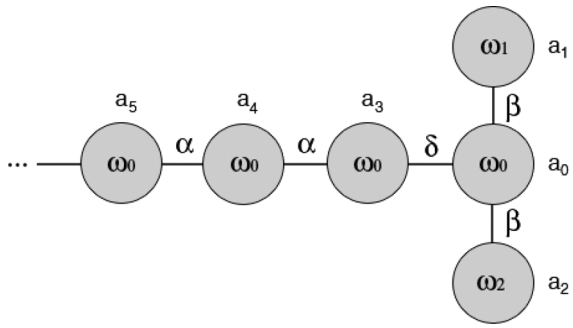

Fig. 2. Three-cavity system coupled to a CROW with coupling constant δ. The three-cavity system coupling constant is β, and the CROW inter-cavity coupling constant is α.

Loss terms (e.g., radiation losses) are ignored in the theory. Section VI contains a brief discussion of the effect of loss. For now we state that loss does not prevent the capture of pulses without reflection. We assume that the amplitudes are normalized such that the energy in cavity m is $|a_m|^2$. The energy in the three-cavity system is

$$U = |a_0|^2 + |a_1|^2 + |a_2|^2. \tag{2}$$

It can be shown that the total energy is conserved by (1). The dynamic tuning process is completely specified by the tuning curves $\omega_1(t)$ and $\omega_2(t)$. We will examine the system's behavior by numerically integrating (1) for different tuning curves.

We assume an input pulse that is Gaussian in time, defined to have field amplitude

$$a(t) = e^{-\frac{t^2}{2T^2}} e^{i\phi(t)} \tag{3}$$

where ϕ is the phase of the pulse. For an unchirped Gaussian pulse, $\phi(t) = \omega_0 t + \phi_0$ for some constant ϕ_0. The width $T = 3\alpha/\delta^2$ is chosen from the optimization process, detailed in Section V. The corresponding intensity in the waveguide is

$$I(t) = v_g e^{-\frac{t^2}{T^2}} \tag{4}$$

where v_g is the waveguide group velocity.

We first consider the pulse dynamics in the static (untuned) system, where $\Delta\omega_1 \equiv \omega_1 - \omega_0 = 0$ and $\Delta\omega_2 \equiv \omega_2 - \omega_0 = 0$, as shown in Fig. 3(a). Fig. 3(b) shows the amplitude in a CROW cavity far from the three-cavity system. The plot shows the incident pulse as well as a reflected pulse of the same magnitude. Fig. 3(c) shows the energy U of the three-cavity system. The energy increases as the pulse reaches the cavities and then decreases as the pulse is reflected in the opposite direction.

We next consider the pulse dynamics in the dynamically tuned system. Fig. 3(d)–(f) show how proper tuning of ω_1 and ω_2 results in the near complete capture of the input pulse. Specifically, we set $\Delta\omega_2(t) = -\Delta\omega_1(t)$ and determine $\Delta\omega_1(t)$ as described later in the text, resulting in the tuning curve shown in Fig. 3(d). Fig. 3(e) shows the amplitude in a CROW cavity near the input. The incident pulse is the same as in Fig. 3(b), but the reflected pulse is absent. The reflected energy is less than 0.01% of the incident energy. Fig. 3(f) shows that the energy of the pulse is almost completely transferred to the three-cavity system. Importantly, energy transfer occurs despite the fact that the spatial extent of the pulse is much larger than the three-cavity system.

The capture process may be understood as the time reversal of the pulse release process shown in Fig. 3(g)–(i). In the release process, the system is initialized with energy stored in the three-cavity system. In Fig. 3(g), the time reverse of the tuning curve in Fig. 3(d) is used. This results in the release of a Gaussian pulse [Fig. 3(h)] that is the time reverse of the pulse that was captured in Fig. 3(d)–(f), and the near complete transfer of energy from the three-cavity system to the waveguide [Fig. 3(i)]. The release process is more straightforward to study numerically than the capture process, and we will devote most of the remainder of this paper to pulse release, bearing in mind that the results will also apply to the time-reversed pulse capture process.

The most important feature of a pulse capturing/releasing system is that it must end/begin in a state that is decoupled from the waveguide, which we refer to as the *dark state*. Capturing light in a dark state has been discussed previously in [4], [10], [11]. The dark state has equal magnitude, opposite sign amplitudes in cavities 1 and 2 and does not leak energy into the waveguide, that is,

$$\begin{aligned} a_2 &= -a_1 \\ a_m &= 0 \quad m \neq 1, 2 \end{aligned} \tag{5}$$

satisfy

$$\frac{d|a_m|}{dt} = 0 \tag{6}$$

for all m in (1). It should be noted that the dark state has infinite lifetime only if the waveguide and cavities are lossless. In the pulse release process, initializing the system in the dark state and tuning ω_1 and ω_2 away from ω_0 allows for a controlled leakage of energy into the waveguide. The particular shape of the output pulse depends on the shape of the tuning curves.

In the dynamic process considered in Fig. 3, we enforced the constraint that $\Delta\omega_2(t) = -\Delta\omega_1(t)$. If instead only one side cavity is tuned, the output pulse is chirped. Fig. 4(a) shows the magnitude of a pulse generated in this manner with the detuning specified in Fig. 4(b). Note the amplitude profile is still Gaussian. However, Fig. 4(c) shows that the instantaneous frequency $d\phi/dt$ of the pulse scales with the detuning. The time reversed tuning scheme thus allows only for the capture of a pulse with identical chirping. In contrast, when both side cavities are tuned with $\Delta\omega_2 = -\Delta\omega_1$, the instantaneous frequency

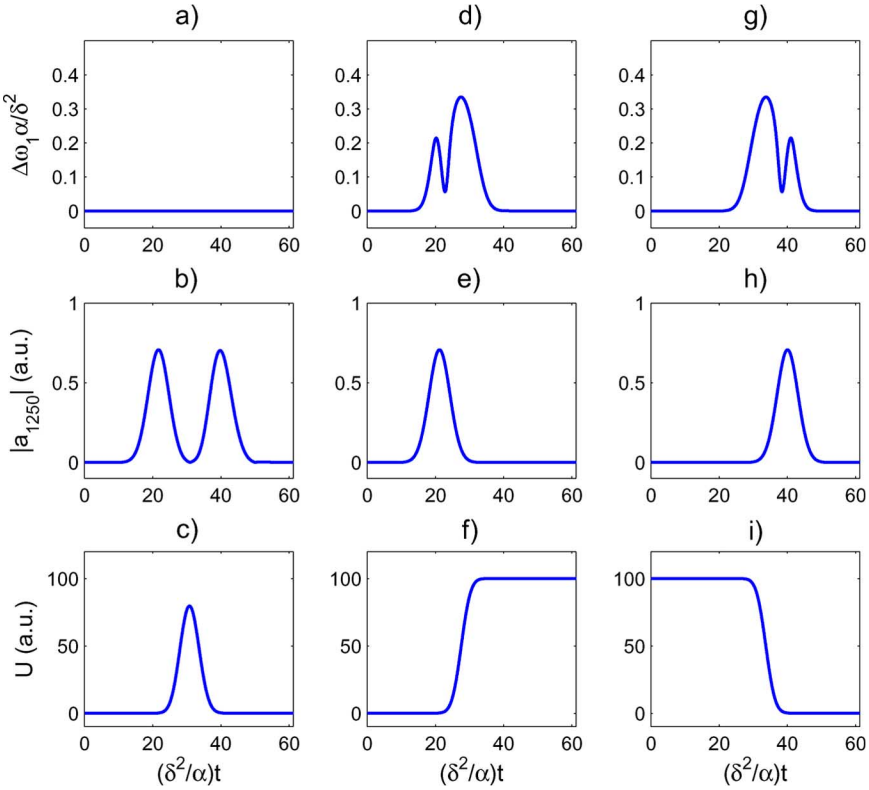

Fig. 3. The temporal behavior of the system shown in Fig. 2 for three different tuning schemes. The system parameters are $\beta = 0.43\delta^2/\alpha$ and $\alpha = 10\delta$. There are 5000 CROW cavities. (a), (d), (g) The tuning curve $\Delta\omega_1 = -\Delta\omega_2$. (b), (e), (h) The amplitude at cavity 1250. (c), (f), (i) The total energy U stored in cavities 0, 1, and 2. (a)–(c) An input pulse with $T = 3\alpha/\delta^2$ is reflected when no tuning is performed. (d)–(f) The same pulse is completely absorbed and there is no reflected pulse when the tuning is optimized. (g)–(i) The time reverse of (d)–(f). The system begins in a stable dark state of the three-cavity system and the time-reversed tuning curve generates a Gaussian pulse.

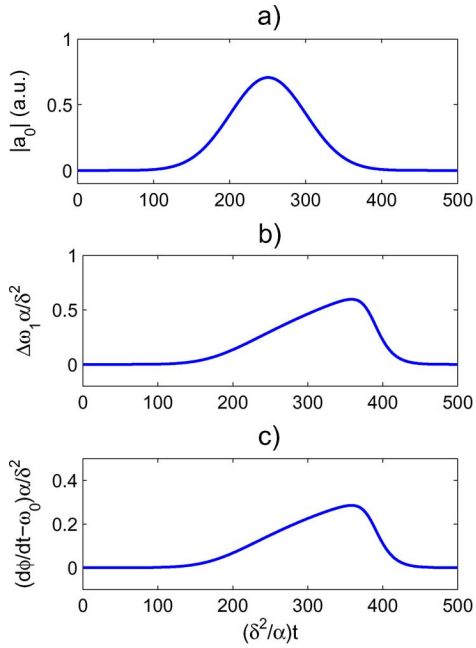

Fig. 4. Generation of a $T = 50\alpha/\delta^2$ chirped Gaussian pulse by tuning a single side cavity. (a) The magnitude of the field amplitude probed at cavity 0. (b) The tuning curve for cavity 1. (c) The instantaneous frequency of the pulse, probed at cavity 0.

is fixed at ω_0 and the time reversed process allows for the capture of an unchirped pulse. This scheme is used in the remainder of the paper.

III. Methods

Here, we present a method for determining the optimal tuning curve for pulse capture and release, given the shape of the input pulse. For a given set of system parameters α, β, δ, and ω_0, we wish to determine the detuning curve $\Delta\omega_1(t) = -\Delta\omega_2(t)$ such that the pulse intensity $I(t)$ in the waveguide has a given shape in the pulse release process. By conservation of energy, $I(t)$ is simply related to the change in energy in the three-cavity system:

$$I(t) = -v_g \frac{dU}{dt}. \tag{7}$$

Let t_i be a particular time in the evolution, and $t_f = t_i + \Delta t$. The parameter Δt is some multiple of the integration time step. Integrating (7) over a time interval $[t_i, t_f]$ gives

$$\int_{t_i}^{t_f} I(t')dt' = -v_g \left(U(t_f) - U(t_i)\right). \tag{8}$$

The left-hand side of (8) is known from the given pulse shape. The right side of (8) depends on the value of $\Delta\omega_1(t)$ in the time interval Δt through (1) and (2). In the time interval in question $\Delta\omega_1(t)$ is approximated by

$$\Delta\omega_1(t) = \Delta\omega_1(t_i) + (t - t_i)\Delta\omega_1'(t_i) \tag{9}$$

where $\Delta\omega_1'$ denotes the time derivative of $\Delta\omega_1$. We choose trial values for $\Delta\omega_1'(t_i)$ and numerically integrate (1) in the interval

using (9) for the detuning. Each trial yields some change in $v_g U$, which can be compared with the left side of (8) to determine the error for the trials. Given these trial values and errors, we apply Newton's method to determine successive trials until the error falls below some threshold. The final value of $\Delta\omega_1'(t_i)$ is used to advance the system to $t_i + \Delta t/S$, where S is a smoothing parameter. Typically we set S equal to 50 and $\Delta t = 1/\gamma$. In this manner we determine the entire tuning curve. The tuning curve will depend on the shape of the output pulse. This method works for arbitrarily shaped pulses (not just Gaussian pulses), provided the instantaneous frequency is constant. It may be the case that at some time step, Newton's method fails to converge, in which case the desired pulse cannot be released and we call $I(t)$ unfeasible. We will discuss the feasible solution space in Section V, but first we will simplify the system and discuss the dynamics in detail.

IV. Dynamics

Above, we have demonstrated pulse capture and release for a particular choice of system parameters and pulse width. This section is devoted to classifying and understanding the different regimes of dynamic behavior observed for various pulse widths T and system parameters β, γ. In Section IV-A we will simplify the system under consideration to make an analytical study feasible. In Section IV-B, we will use this framework to develop an adiabatic approximation in which the dynamics are described in a particularly simple manner. We derive conditions for the validity of the adiabatic approximation which correspond to the weak waveguide coupling, low bandwidth limit. In Section IV-C we will explore what happens when higher bandwidth pulses are released and the adiabatic approximation breaks down.

A. Reduced Equations of Motion

Thus far we have considered the particular case of three cavities coupled to a CROW. In practice many other varieties of waveguide may be used. Therefore, we are interested in the physical aspects of the pulse release system that are independent of the particular choice of waveguide. A simplified model of our system is shown in Fig. 1. The cavity system is coupled to an external waveguide mode with a coupling constant γ.

The system in Fig. 1 is described by a symmetric, non-Hermitian 3×3 matrix,

$$C = \begin{pmatrix} \omega_0 + i\gamma & \beta & \beta \\ \beta & \omega_1 & 0 \\ \beta & 0 & \omega_2 \end{pmatrix} \tag{10}$$

where

$$\frac{da_j}{dt} = iC_{jm}a_m. \tag{11}$$

Summation over repeated indexes is implied. Note that the waveguide coupling constant γ shows up as an effective loss in cavity 0. We may eliminate the dependence on ω_0 by defining amplitudes

$$A_m(t) = exp(-i\omega_0 t)a_m(t). \tag{12}$$

We may also define a dimensionless time $\tau = \gamma t$. Using the relations $\Delta\omega_1 = \omega_1 - \omega_0$ and $\Delta\omega_2 = -\Delta\omega_1$, (10) and (11) become

$$\begin{aligned} D &= D_0 + \frac{\Delta\omega_1}{\gamma} D_1 \\ &\equiv \begin{pmatrix} i & \frac{\beta}{\gamma} & \frac{\beta}{\gamma} \\ \frac{\beta}{\gamma} & 0 & 0 \\ \frac{\beta}{\gamma} & 0 & 0 \end{pmatrix} + \frac{\Delta\omega_1}{\gamma} \begin{pmatrix} 0 & 0 & 0 \\ 0 & 1 & 0 \\ 0 & 0 & -1 \end{pmatrix} \end{aligned} \tag{13}$$

and

$$\frac{dA_j}{d\tau} = iD_{jm}A_m. \tag{14}$$

It is easy to see from the form of D that the dynamics will depend only on the dimensionless ratios β/γ and $\Delta\omega_1/\gamma$ and the dimensionless pulsewidth γT.

B. Adiabatic Dynamics

We will show that in the adiabatic limit, the system is described by the evolution of a single state that continuously evolves from the initial dark state. We follow a treatment of the adiabatic approximation commonly made in quantum mechanics with a Hermitian system matrix [16]. We will first derive a simple condition for the validity of the adiabatic approximation in the limit where the three-cavity system is weakly coupled to the waveguide. Although our system is non-Hermitian, we find that the results are similar to the Hermitian case. We will then describe how the dynamics are simplified when this adiabatic condition is satisfied.

We begin by diagonalizing D at each time τ:

$$D = S\Lambda S^{-1}. \tag{15}$$

The τ dependence is suppressed for clarity. Here S is the matrix of eigenvectors, and $\Lambda = diag(\lambda_k)$, $k = 0 \ldots 2$ is the eigenvalue matrix of D. The eigenvectors are defined up to an arbitrary scaling factor. We project the amplitudes A_m onto the time-dependent basis of instantaneous eigenstates

$$V_k = (S^{-1})_{km}A_m. \tag{16}$$

Henceforth, the $k = 0$ eigenstate will refer to the eigenstate that evolves from the initial dark state, and the $k \neq 0$ eigenstates will refer to the other initially unoccupied states. We now introduce the evolution operator W defined by

$$V(\tau) = W(\tau)V(0) \tag{17}$$

By differentiating with respect to τ, we find that

$$\frac{dW}{d\tau} = i\left(\Lambda - S^{-1}\frac{dS}{d\tau}\right)W = i(\Lambda - \Gamma)W \tag{18}$$

where $\Gamma \equiv S^{-1}dS/d\tau$. The Γ matrix is nondiagonal and couples the instantaneous eigenstates. The form of Γ can be simplified by fixing the scale of the eigenstates such that the time derivative of the jth eigenstate has no j component

$$\left(S^{-1}\frac{dS}{d\tau}\right)_{jj} = 0. \tag{19}$$

No summation is implied in (19). This condition can always be met, provided S is nonsingular. We may then apply time independent perturbation theory to D with a perturbation $\delta\omega D_1$, yielding an exact value for the time derivative of the eigenstates. This allows us to write Γ as

$$\Gamma_{jk} = \begin{cases} \frac{\left(\frac{d\Delta\omega_1}{d\tau}/\gamma\right)(S^{-1}D_1S)_{jk}}{\lambda_{kj}}, & j \neq k \\ 0, & j = k \end{cases} \tag{20}$$

where

$$\lambda_{kj} \equiv \lambda_k - \lambda_j. \tag{21}$$

The adiabatic approximation consists of ignoring Γ, so that an eigenstate of $D(0)$ at time 0 evolves, in time τ, to the corresponding eigenstate of $D(\tau)$, with a change in amplitude and phase due to the Λ term alone.

In order to determine the region of validity for the adiabatic approximation, we first isolate the effect of Γ by introducing $\tilde{W}$, the solution of (18) in the absence of Γ

$$\frac{d\tilde{W}}{d\tau} = i\Lambda\tilde{W} \tag{22}$$

with formal solution

$$\tilde{W}(\tau) = \exp\left(\int_0^\tau \Lambda(\tau')d\tau'\right). \tag{23}$$

Now define

$$X = \tilde{W}^{-1}W \tag{24}$$

which satisfies

$$\frac{dX}{d\tau} = i\bar{\Gamma}X \tag{25}$$

where

$$\bar{\Gamma} = \tilde{W}^{-1}\Gamma\tilde{W}. \tag{26}$$

In integral form, with appropriate initial conditions, (25) becomes

$$X(\tau) = 1 + i\int_0^\tau \bar{\Gamma}(\tau')X(\tau')d\tau'. \tag{27}$$

This equation provides a perturbative solution for $X(\tau)$. To determine the condition for validity of the adiabatic approximation, we solve (27) to first order in $\bar{\Gamma}$ to obtain

$$X(\tau) \approx 1 + i\int_0^\tau \bar{\Gamma}(\tau')d\tau'. \tag{28}$$

If the system is initially in eigenstate 0, i.e., $V_k(0) = \delta_{k0}$, then (23), (24), (26), and (28) yield, for $k \neq 0$,

$$V_k(\tau) = i\exp\left(i\int_0^\tau \lambda_k(\tau')d\tau'\right) \times \int_0^\tau \Gamma_{k0}(\tau')\exp\left(i\int_0^{\tau'} \lambda_{0k}(\tau'')d\tau''\right)d\tau' \tag{29}$$

and for $k = 0$

$$V_0(\tau) = \exp\left(i\int_0^\tau \lambda_0(\tau')d\tau'\right). \tag{30}$$

Thus far, we have made no reference to the form of the dynamics, and (29) and (30) hold for any system, Hermitian or not. The system under consideration is non-Hermitian, but it is instructive to consider the weak waveguide coupling limit $\beta/\gamma \to \infty$ in which case the system is Hermitian. In this case, S is unitary and the scale of the eigenvectors is constant. A measure of error introduced by the adiabatic approximation is given, to first order, by the ratio κ of the amplitude in a state $k \neq 0$ to the amplitude in the state $k = 0$

$$\kappa = \left|\exp\left(i\int_0^\tau \lambda_{k0}(\tau')d\tau'\right) \times \int_0^\tau \Gamma_{k0}(\tau')\exp\left(i\int_0^{\tau'} \lambda_{0k}(\tau'')d\tau''\right)d\tau'\right|. \tag{31}$$

The condition for validity of the approximation can now be written as $\kappa \ll 1$ for all $k \neq 0$.

We can simplify this condition further. By examining the characteristic equation for D for arbitrary $\Delta\omega_1/\gamma$, we can bound λ_{k0} from below by β/γ. We may also bound the numerator of Γ_{k0} in (20) from above by $2(d\Delta\omega_1/d\tau)/\gamma$, as S is unitary and so the maximum magnitude of any matrix entry of S or $S^{-1} = S^\dagger$ is 1. Using these bounds, and noting that λ_{k0} is real, we have from (20) and (31)

$$\kappa \leq \left|\int_0^\tau 2\frac{d\Delta\omega_1}{d\tau'}\frac{1}{\beta}d\tau'\right| \tag{32}$$

so that a sufficient condition for validity of the adiabatic approximation, in the Hermitian case, is

$$\frac{\Delta\omega_{1_{\max}}}{\beta} \ll \frac{1}{2}. \tag{33}$$

We find empirically that, for long pulses with $\gamma T \gg 1$, the tuning curve $\Delta\omega_1(\tau)$ that is generated using (7)–(9) always satisfies the condition of (33). Thus, narrow-bandwidth pulses can be captured using adiabatic dynamics, provided we work with

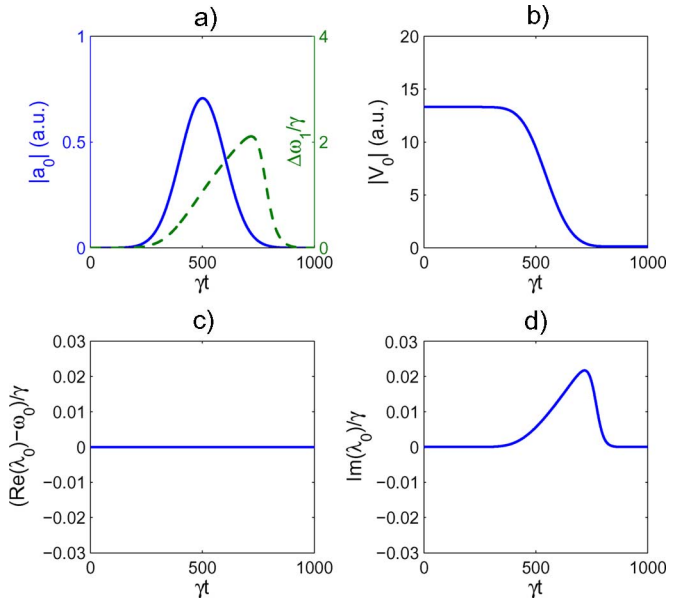

Fig. 5. The evolution of the eigenstate descended from the dark state, with system parameters $\beta/\gamma = 10, \gamma T = 100$. (a) The tuning curve (dashed line) and the amplitude of the generated pulse, probed at cavity 0 (solid line). (b) The magnitude of the amplitude in the $k = 0$ eigenstate, $|V_0|$. (c) The real part of λ_0, corresponding to the eigenfrequency. (d) The imaginary part of λ_0, proportional to the leakage rate.

systems with $\beta/\gamma \gg 1$ so that the Hermitian assumption is appropriate.

The dynamics in the adiabatic regime can be described with a single time-dependent eigenvalue $\lambda_0(\tau)$. The Γ term in (18) can be ignored, and we have

$$\frac{dV_0}{d\tau} = i\lambda_0(\tau)V_0. \tag{34}$$

All of the energy U of the system is contained in this single adiabatically evolving state. The dynamics are similar to those for macroscopic mirror, single-cavity pulse capture [12]. The difference is in the method of controlling the leakage rate of the cavity.

Fig. 5 illustrates the dynamics for a typical adiabatic pulse release, with $\beta/\gamma = 10$ and $\gamma T = 100$. Fig. 5(a) shows the tuning curve (dashed line) and the resulting output pulse (solid line). The tuning increases monotonically until most of the pulse energy has been released, at which point it decreases to zero. Fig. 5(b) shows the magnitude of the amplitude in the dark state, which decreases monotonically with time. In the adiabatic approximation, this quantity is equal to the square root of the energy in the three-cavity system. Fig. 5(c) shows the real part of λ_0. We see this value is always zero. As a result, the instantaneous frequency of the output pulse is fixed at ω_0. Fig. 5(d) shows the imaginary part of λ_0, which is proportional to the leakage rate of the eigenstate into the waveguide, μ. The leakage rate increases for most of the pulse release time and then decreases to zero.

The tuning curve for adiabatic pulse release may be determined in a simple manner as follows. It can be shown that for small $\Delta\omega_1/\beta$ we have

$$\mu/\gamma = 2\mathrm{Im}(\lambda_0/\gamma) \approx (\Delta\omega_1/\beta)^2. \tag{35}$$

The intensity $I(\tau)$ of the output pulse is proportional to μ/γ times the energy $U(\tau)$ remaining in the system. $U(\tau)$ is related to $I(\tau)$ by (7). Thus, μ/γ is fixed by $I(\tau)$ alone, and we can determine $\Delta\omega_1(\tau)$ from μ/γ and (35), without resorting to the numerical methods of Section III.

If γ is of the same order as β, we can no longer analytically derive a condition analogous to (33) for the validity of the adiabatic approximation. In particular, the eigenvalues are not real and S is not unitary or nonsingular, so it is difficult to set useful analytic bounds on Γ. However, we find numerically that the bounds we discovered in the Hermitian case actually hold for the non-Hermitian system as well, provided $\beta/\gamma \gtrsim 0.5$. Adiabatic behavior, in which a single state dominates the process, is observed for even lower β/γ provided γT is sufficiently large. The condition (33), although derived under the assumption that the system is Hermitian, is adequate for predicting this behavior.

C. Nonadiabatic Dynamics

For many applications, it is useful to maximize the bandwidth of the captured pulse. However, for large bandwidth (small γT), the adiabatic approximation breaks down, and the pulse dynamics no longer satisfy (33). Several subtleties emerge in the study of the instantaneous eigensystem of D in the nonadiabatic case. First, we can no longer ignore coupling between eigenstates. The initial dark state will transfer energy to the other two eigenstates through the Γ term in (18). These other eigenstates will in general have different frequencies and decay rates. Furthermore, as D is non-Hermitian, the eigenvector matrix S is nonunitary and the total energy in the system

$$U = A^\dagger A = V^\dagger S^\dagger S V \neq V^\dagger V. \tag{36}$$

The cross terms of $S^\dagger S$ prevent us from interpreting the individual $|V_k|^2$ as energies. This also implies that the imaginary parts of the eigenvalues are not strictly proportional to energy leakage rates from the corresponding eigenstates.

There is another nonadiabatic regime distinct from the small γT regime, which occurs when the non-Hermitivity of D becomes important. Specifically, when $\beta/\gamma \lesssim 0.385$, there exists a critical value of $\Delta\omega_1/\gamma$ at which S becomes singular, $\Gamma \to \infty$, and the adiabatic approximation breaks down. For certain values of γT, the solution for $\Delta\omega_1/\gamma$ crosses this critical point. The $k = 0$ eigenstate becomes indistinguishable from one of the $k \neq 0$ eigenstates. The frequencies of these two states (i.e., the real part of the eigenvalues of C in (10) split symmetrically from ω_0, while the frequency of the third eigenstate remains fixed at ω_0. In other cases the frequencies begin symmetrically split, and diverge or reconverge during the tuning process, depending on the value of β/γ.

We demonstrate the behavior of the system in the two nonadiabatic regimes. Fig. 6 illustrates the typical behavior of the system in the high-bandwidth (small γT) regime. The example shows a system with $\beta/\gamma = 0.43$ releasing a pulse of width $\gamma T = 3$. Fig. 5 shows the tuning curve (dashed line) and released pulse (solid line). Fig. 6(b)–(d) show the magnitude of the amplitudes in the eigenstates (V_k), the real part of the eigenvalues, and the imaginary part of the eigenvalues, respectively. In (b)–(d), the solid line corresponds to the $k = 0$ eigenstate.

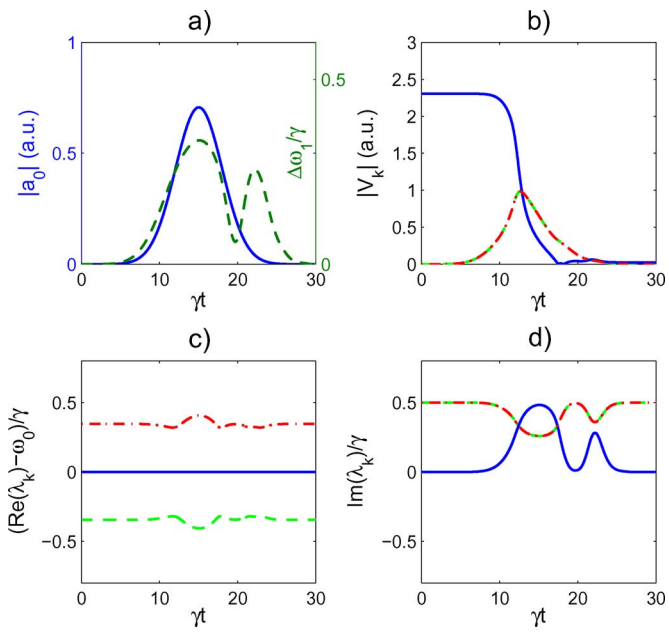

Fig. 6. Nonadiabatic evolution of the three eigenstates in the small γT regime. The solid line corresponds to the $k = 0$ eigenstate in (b)–(d). The system parameters are $\beta/\gamma = 0.43, \gamma T = 3$. (a) The tuning curve (dashed line) and the amplitude of the generated pulse, probed at cavity 0 (solid line). (b) The magnitude of the amplitude in the eigenstates, $|V_k|$. (c) The real part of λ_k, corresponding to the eigenfrequency. (d) The imaginary part of λ_k.

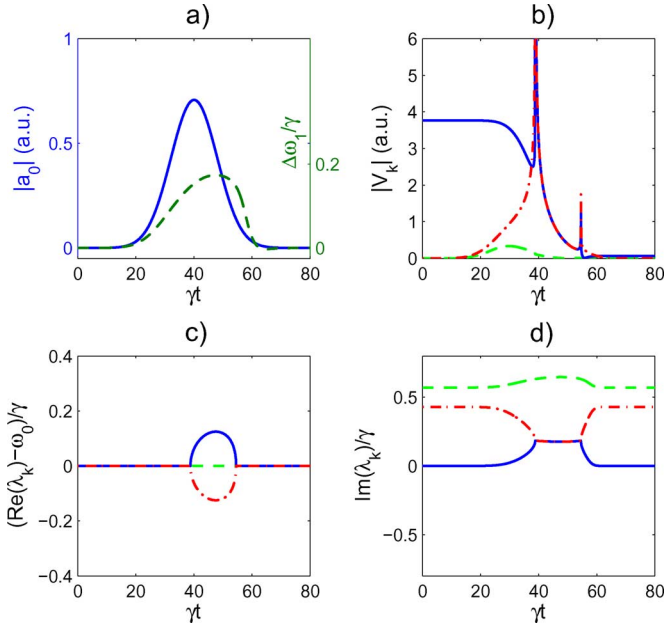

Fig. 7. The nonadiabatic evolution of the three eigenstates in the small β/γ regime. The system parameters are $\beta/\gamma = 0.35, \gamma T = 8$. (a) The tuning curve (dashed line) and the amplitude of the generated pulse, probed at cavity 0 (solid line). (b) The magnitude of the amplitude in the eigenstates, $|V_k|$. (c) The real part of λ_k, corresponding to the eigenfrequency. (d) The imaginary part of λ_k.

We see in Fig. 6(b) that significant amplitude accumulates in all three eigenstates over the course of the tuning process. In Fig. 6(c), we observe that the $k = 0$ state is centered at ω_0, while the other two states have symmetrically split frequencies. The symmetrically split states have identical imaginary parts of their eigenvalues, as seen in Fig. 6(d). This implies that the output will have fixed instantaneous frequency ω_0, which is a general property enforced by the anti-symmetric detuning of cavities 1 and 2. The oscillation in the detuning curve in Fig. 6(a) may be understood as a result of a beating phenemonon introduced by having two states contributing at frequencies split symmetrically from ω_0.

Fig. 7 demonstrates the behavior of the system in the second nonadiabatic regime, where the non-Hermitivity of the system matrix place a particularly important role. Fig. 7(a) shows the tuning curve and released pulse for $\beta/\gamma = 0.35 < 0.385$ and $\gamma T = 8$. Since γT is larger than in the system illustrated by Fig. 6, one might expect the behavior to be more like the adiabatic case. In particular, one might expect less amplitude in the $k \neq 0$ states relative to the amplitude in the $k = 0$ state. Instead, *more* amplitude accumulates in one of the $k \neq 0$ states. Fig. 7(b) shows the eigenstate amplitudes. One of the $k \neq 0$ states grows in amplitude to equal the $k = 0$ state, and both amplitudes diverge near $\gamma t = 40$. The divergence occurs because the eigenstates are no longer linearly independent, which occurs as S becomes singular and $\Gamma \to \infty$. This behavior is unique to non-Hermitian systems. In such systems, the eigenstates are not orthogonal, so the modal amplitudes do not correspond to energies. Despite this divergence in modal amplitude, the energy does not diverge, and in fact follows the same trajectory as in Fig. 3. At the time of the divergence, the real parts of the eigenstate frequencies split, as shown in Fig. 7(c). At slightly later times, both amplitudes are equal. Another divergence is observed in the amplitudes near $\gamma t \approx 55$, where the split frequencies reconverge. Fig. 7(d) shows the imaginary parts of the eigenvalues. During the time that the real parts of the eigenvalues are split, the imaginary parts of the eigenvalues of the split states are equal, again fixing the instantaneous frequency of the output pulse at ω_0.

V. Bandwidth Optimization

Having characterized the dynamics of the system, we now determine the attainable pulse bandwidth, given some maximum available detuning. For each value of β/γ and each feasible output pulsewidth γT, define a figure of merit

$$F = \frac{B}{\Delta\omega_{1_{\max}}} = \frac{1/(\gamma T)}{\Delta\omega_{1_{\max}}/\gamma} \tag{37}$$

where $B = 1/T$ is the bandwidth of the output pulse, and $\Delta\omega_{1_{\max}}$ is the peak detuning. Defining a peak detuning requires care, as the detuning required to generate a perfect Gaussian pulse will diverge as $t \to \infty$. There are several ways to address this issue. One could choose a time period of interest during which any deviation from a Gaussian amplitude is considered unacceptable. Outside this region one could clamp the detuning and allow for distortion of the pulse. The problem with this method is that the peak detuning is very sensitive to the arbitrary region chosen. Furthermore, it is difficult to quantify the error introduced. In our approach, we eliminate the divergence in the detuning by allowing some small fraction of the energy

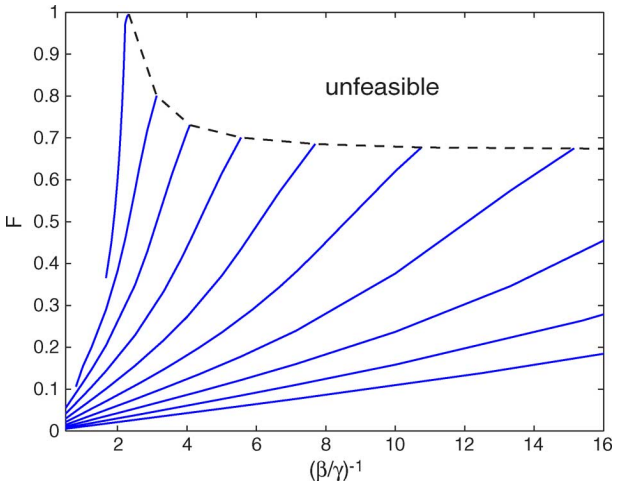

Fig. 8. Figure of merit as a function of $(\beta/\gamma)^{-1}$ for (left to right) $\gamma T = 3$, 8, 16, 32, 64, 128, and 256. The dashed line denotes the calculated boundary of the feasible solution space.

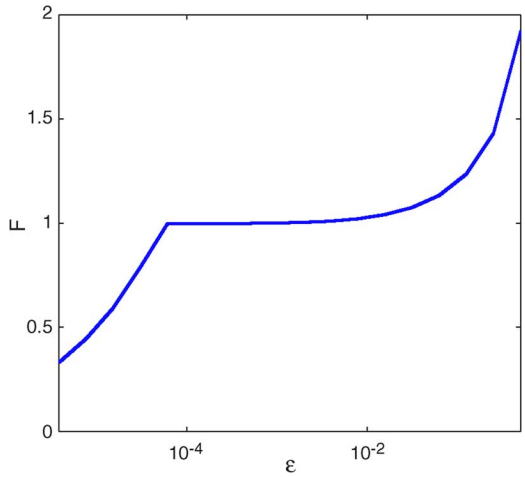

Fig. 9. Figure of merit as a function of ϵ for $\beta/\gamma = 0.43, \gamma T = 3$.

in the cavities to remain unreleased, that is, we solve for the detuning required to release a pulse with intensity

$$I(t) = (1-\epsilon) I_0 e^{-\frac{t^2}{T^2}} \tag{38}$$

for some small ϵ. Numerical experiments demonstrate that if a pulse is captured with the time reversed tuning curve, a similar fraction of the incident energy is reflected. In this manner we may control the desired capture efficiency. We set $\epsilon = 10^{-4}$ in all numerical experiments we have discussed.

With this same value of ϵ, Fig. 8 shows the figure of merit as a function of $(\beta/\gamma)^{-1}$ for various values of γT. F increases with increasing $(\beta/\gamma)^{-1}$ and decreasing γT. The trend $F \propto (\beta/\gamma)^{-1}$ for fixed γT can be understood in the adiabatic case as follows. For Gaussian pulses, the maximum required leakage rate is proportional to $(\gamma T)^{-1}$. On the other hand, in the adiabatic approximation, the leakage rate is directly proportional to imaginary part of the $k = 0$ eigenvalue, which for small $\Delta\omega_1/\beta$ is approximately proportional to $(\Delta\omega_1/\beta)^2$, as in (35). Using these two relations, we find

$$F \propto (\gamma T)^{-\frac{1}{2}} (\beta/\gamma)^{-1}. \tag{39}$$

This trend is roughly followed in the nonadiabatic regime as well.

The dotted line in Fig. 8 marks the boundary of the feasible solution space. The minimum width γT for a given value of β/γ scales as $(\beta/\gamma)^{-2}$ for sufficiently large γT. This follows from (39), which is approximately valid in the nonadiabatic regime, and the assumption of a maximal F independent of γT. For small γT, this trend is violated, and higher values of F are attained. The optimal figure of merit $F \approx 1.0$ is obtained with $\gamma T \approx 3$ and $\beta/\gamma \approx 0.43$. The dynamic behavior of this optimal system was shown in Fig. 6. The system parameters are the very same we saw implemented with the CROW system in Fig. 3, with $\delta = 10\gamma$ and $\alpha = 100\gamma$.

Fig. 9 shows the ϵ dependence of F at this optimal point. We see F is roughly independent of ϵ in the range $\epsilon = 10^{-4} - 10^{-2}$. If the requirements on ϵ are very stringent, F decreases. On the other hand, if only a small portion of the pulse must be captured, higher bandwidths may be attained.

VI. Concluding Remarks

We have described a dynamically tuned few-resonator system capable of capturing and releasing light pulses. This system could be used as the basis of a unidirectional buffer, shown in Fig. 10. The three-cavity system is coupled to two waveguides, one for pulse capture and one for release. Each waveguide is gated by an additional side cavity, which acts as a mirror when the cavity resonant frequency is tuned to the carrier frequency in the waveguide. The operation would be as follows. Initially, the input gate resonator is tuned far from the carrier frequency, and the output gate resonator is tuned to the carrier frequency. In this case the transmission from the capture waveguide into the three-cavity system is near unity at the carrier frequency, while the transmission from the three-cavity system into the exit waveguide is zero at the carrier frequency. The three-cavity system may then be tuned appropriately to capture a pulse. Once the pulse is captured, the input and output gate resonators are tuned in the opposite manner such that the transmission into the entrance waveguide is zero and the transmission into the exit waveguide is near unity. The pulse may then be released from the three-cavity system into the exit waveguide by carrying out the time reverse of the capture tuning process.

Finally, we will comment on the practical requirements for experimental implementation of our pulse capture and release system. We assume that the resonant frequencies of the cavities are tuned by modulating the index of refraction. In a 2-D photonic crystal, cavities may be created by introducing defects in a triangular lattice of air holes in a silicon slab, and the index of refraction near the cavity can be tuned by carrier injection. Current technology limits the maximum index change to $\Delta n/n \approx 10^{-4} - 10^{-3}$. Assuming the fractional change in resonant frequency is directly related to the fractional change in index of refraction, $\Delta\omega_1/\omega_0 \approx \Delta n/n$, and assuming a system with optimal system parameters such that $F \approx 1$, the shortest pulse that can be captured at a 200-THz carrier frequency has $T \sim$1-10 ps.

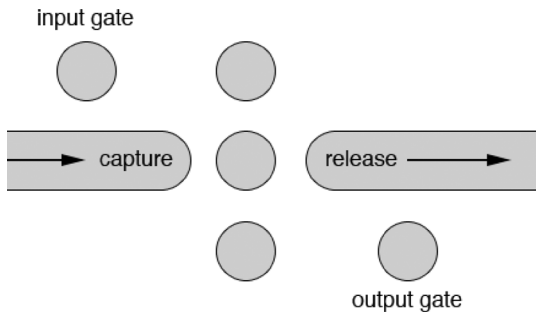

Fig. 10. Schematic of a unidirectional buffer utilizing the three-cavity system. Two side cavities gate the input and output of the system.

The coupling constants required for implementing the capture of a 10-ps pulse may be calculated assuming an optimal design with $\gamma T = 3$, $\beta/\gamma = 0.43$. This yields values of $\gamma = 3 \times 10^{11} s^{-1} = 4.2 \times 10^{-4}(c/a)$, $\beta = 1.3 \times 10^{11} s^{-1} = 1.8 \times 10^{-4}(c/a)$ for a photonic crystal implementation with lattice constant $a = 420$ nm [11]. These values correspond to Q factors of $Q_\gamma \approx 2000$, $Q_\beta \approx 5000$. If smaller coupling constants (larger Q) are chosen, the minimum width T of a pulse which can be captured will increase. Intercavity coupling and and waveguide-cavity coupling in photonic crystals have been studied extensively [13], [17]–[19]. The required coupling constants should present no difficulties for practical implementation. For example, by spacing L3 cavities four lattice constants ($a = 420$ nm) apart, the appropriate value of $\beta \approx 3 \times 10^{11} s^{-1}$ may be achieved [17]. Regarding cavity-waveguide coupling, values of Q_γ as low as 500 have been demonstrated [19]. Exponentially weaker coupling, appropriate for capturing longer pulses, may be achieved by increasing the distance between cavities.

Other factors limiting the system are the timescales for tuning and loss. The timescale for optical free carrier injection is set by the free carrier lifetime in silicon photonic crystal structures. Typical carrier lifetimes for photonic crystal microcavities are on the order of 100 ps [20], and this value may be further reduced to ~70 ps using techniques such as ion-implantation [21]. It may also be possible to modulate cavities at a time scale shorter than the carrier recombination scale by the use of reverse bias schemes that drive the carriers out of the tuning region [22]. It should be noted that in our anti-symmetric tuning scheme we require positive tuning of one cavity and negative tuning of the other. This negative tuning may be implemented by designing the cavities to have different resonant frequencies before tuning is carried out. A positive bias signal may be applied to one of the cavities to tune them to the same resonant frequency. The negative tuning may then be carried out by reducing this positive bias signal.

The cavity lifetime limits the holding time of pulses in the system. State of the art cavities have a lifetime of approximately 1 ns [23]. In conjunction with the lower limit set by the tuning timescale, this leaves a window between 100 ps and 1 ns for practical operation, roughly corresponding to bandwidths between 100 MHz and 1 GHz. In the presence of a uniform cavity loss rate η, the system is still capable of capturing pulses without reflection. It can be shown that for Gaussian pulses, the required tuning curve is simply time shifted by ηT^2 when loss is present. This has been verified by including uniform cavity loss terms in the coupled mode theory simulations. There is thus no limit on the width of the pulses which can be captured or released. In principle, then, very high field energies may be obtained in the cavities with low pulse power, which suggests applications in nonlinear signal processing. The peak amplitude in the cavities and the amplitude of released pulses is reduced by loss. For holding times t_h long compared to the pulsewidth T, the released amplitude will scale exponentially as $\exp(-\eta t_h)$. These results have been confirmed with coupled mode theory simulations.

In summary, we have described a few-cavity system capable of capturing light pulses with negligible reflection. We found that when the system is weakly coupled to a waveguide, low-bandwidth operation is well described by the adiabatic evolution of a single state of the system. Very high spatial compression of incident pulses, and consequently, very high nonlinearity enhancement, may be achieved in this regime. In contrast, we found that to achieve the highest bandwidths, relatively high waveguide coupling is required, and multiple states of the system are occupied at once, resulting in complicated dynamics and detuning curves. A simple numerical method was presented which provides the required detuning curve in any case, allowing operation in the high-bandwidth, nonadiabatic regime. The system we describe should be useful for both optical buffering and applications which rely on nonlinearity enhancement.

REFERENCES

[1] M. Soljačić and J. D. Joannopoulos, "Enhancement of nonlinear effects using photonic crystals," *Nat. Mater.*, vol. 3, pp. 211–219, 2004.
[2] M. F. Yanik, S. Fan, and M. Soljačić, "High-contrast all-optical bistable switching in photonic crystal microcavities," *Appl. Phys. Lett.*, vol. 83, pp. 2739–2741, 2003.
[3] M. F. Yanik and S. Fan, "Stopping light all optically," *Phys. Rev. Lett.*, vol. 92, no. 8, p. 083901, Feb. 2004.
[4] M. F. Yanik, W. Suh, Z. Wang, and S. Fan, "Stopping light in a waveguide with an all-optical analogue of electromagnetically induced transparency," *Phys. Rev. Lett.*, vol. 93, p. 233903, 2004.
[5] S. Sandhu, M. L. Povinelli, M. F. Yanik, and S. Fan, "Dynamically tuned coupled-resonator delay lines can be nearly dispersion free," *Opt. Lett.*, vol. 31, no. 13, pp. 1985–1987, Jul. 2006.
[6] S. Sandhu, M. L. Povinelli, and S. Fan, "Stopping and time reversing a light pulse using dynamic loss tuning of coupled-resonator delay lines," *Opt. Lett.*, vol. 32, no. 22, pp. 3333–3335, Nov. 2007.
[7] Z. S. Yang, N. H. Kwong, R. Binder, and A. L. Smirl, "Distortionless light pulse delay in quantum-well Bragg structures," *Opt. Lett.*, vol. 30, no. 20, pp. 2790–2792, Oct. 2005.
[8] J. Khurgin, "Adiabatically tunable optical delay lines and their performance limitations," *Opt. Lett.*, vol. 30, no. 20, pp. 2778–2780, Oct. 2005.
[9] J. B. Khurgin, "Slowing and stopping photons using backward frequency conversion in quasi-phase-matched waveguides," *Phys. Rev. A*, vol. 72, p. 023810, 2005.
[10] Q. Xu, P. Dong, and M. Lipson, "Breaking the delay-bandwidth limit in a photonic structure," *Nat. Phys.*, vol. 3, pp. 406–410, 2007.
[11] Y. Tanaka, J. Upham, T. Nagashima, T. Sugiya, T. Asano, and S. Noda, "Dynamic control of the Q factor in a photonic crystal nanocavity," *Nat. Mater.*, vol. 6, pp. 862–865, 2007.
[12] B. P. J. Bret, T. L. Sonnemans, and T. W. Hijmans, "Capturing a light pulse in a short high-finesse cavity," *Phys. Rev. A*, vol. 68, p. 023807, 2003.
[13] M. Notomi, T. Tanabe, A. Shinya, E. Kuramochi, H. Taniyama, S. Mitsugi, and M. Morita, "Nonlinear and adiabatic control of high-Q photonic crystal nanocavities," *Opt. Exp.*, vol. 15, pp. 17 458–17 481, 2007.

[14] N. Stefanou and A. Modinos, "Impurity bands in photonic in photonic insulators," *Phys. Rev. B*, vol. 57, p. 12127, May 1997.
[15] A. Yariv, Y. Xu, R. K. Lee, and A. Scherer, "Coupled-resonator optical waveguide: A proposal and analysis," *Opt. Lett.*, vol. 24, p. 711, 1999.
[16] A. Messiah, *Quantum Mechanics*. Amsterdam, The Netherlands: North-Holland, 1962, vol. II.
[17] M. L. Povinelli and S. Fan, "Radiation loss of coupled-resonator waveguides in photonic-crystal slabs," *Appl. Phys. Lett.*, vol. 89, p. 191114, 2006.
[18] D. O'Brien, M. D. Settle, T. Karle, A. Michaeli, M. Salib, and T. F. Krauss, "Coupled photonic crystal heterostructure nanocavities," *Opt. Exp.*, vol. 15, p. 1228, 2007.
[19] A. Faraon, E. Waks, D. Englund, I. Fushman, and J. Vučković, "Efficient photonic crystal cavity-waveguide couplers," *Appl. Phys. Lett.*, vol. 90, p. 073102, 2007.
[20] T. Tanabe, M. Notomi, A. Shinya, S. Mitsugi, and E. Kuramochi, "Fast bistable all-optical switch and memory on a silicon photonic crystal on-chip," *Opt. Lett.*, vol. 30, no. 19, p. 2575, 2005.
[21] T. Tanabe, K. Nishiguchi, A. Shinya, E. Kuramochi, H. Inokawa, and M. Notomi, "Fast all-optical switching using ion-implanted silicon photonic crystal nanocavities," *Appl. Phys. Lett.*, vol. 90, p. 031115, 2007.
[22] M. Lipson, "Guiding, modulating, and emitting light on silicon—Challenges and opportunities," *J. Lightw. Technol.*, vol. 23, no. 12, pp. 4222–4238, Dec. 2005.
[23] Y. Takahashi, H. Hagino, Y. Tanaka, B. S. Song, T. Asano, and S. Noda, "High-Q nanocavity with a 2-ns photon lifetime," *Opt. Exp.*, vol. 15, pp. 17 206–17 213, 2007.

Clayton Ryan Otey received the B.S. degree in physics from the California Institute of Technology, Pasadena. He is currently working toward the M.S. degree in applied physics at Stanford University, Stanford, CA.

His research interests include photonic crystals, dynamic photonic structures, and computational electromagnetism.

Michelle L. Povinelli received the B.A. degree (with honors) from the University of Chicago, Chicago, IL, in 1997, the M.Phil. degree from the University of Cambridge, Cambridge, U.K., in 1998, and the Ph.D. degree from the Massachusetts Institute of Technology (MIT), Cambridge, in 2004, all in physics.

She was a Postdoctoral Researcher with the Department of Electrical Engineering, Stanford University, Stanford, CA. She is currently an Assistant Professor with the Ming Hsieh Department of Electrical Engineering, University of Southern California, Los Angeles. Her research area is optics and photonics, specializing in photonic crystals. She has coauthored over 20 refereed journal articles and holds two U.S. Patents.

Dr. Povinelli was awarded several graduate fellowships for her doctoral work, including the Lucent Technologies GRPW Fellowship, the National Science Foundation Graduate Fellowship, the MIT Karl Taylor Compton Fellowship, and the Churchill Fellowship, an award that is given to ten American students per year to study at the University of Cambridge, U.K. In 2006, she was selected as one of five national recipients of a $20,000 L'Oréal For Women in Science Postdoctoral Fellowship grant.

Shanhui Fan (SM'06) received the Ph.D. degree in theoretical condensed matter physics from the Massachusetts Institute of Technology (MIT), Cambridge, in 1997.

He is currently an Associate Professor of electrical engineering with Stanford University, Stanford, CA, and was a Research Scientist with the Research Laboratory of Electronics at MIT prior to his appointment at Stanford. His research interests are in computational and theoretical studies of solid state and photonic structures and devices, especially photonic crystals, microcavities, and nanophotonic circuits and elements. He has published over 150 refereed journal articles, has given over 110 invited talks, and holds 33 U.S. patents.

Dr. Fan is a Fellow of the Optical Society of America (OSA) and a member of the American Physical Society and SPIE. He was the recipient of a National Science Foundation Career Award (2002), a David and Lucile Packard Fellowship in Science and Engineering (2003), the National Academy of Sciences Award for Initiative in Research (2007), and the Adolph Lomb Medal from the OSA (2007).